Journal of Oceanology and Limnology
Vol. 39 No. 3, P. 800-813, 2021
https://doi.org/10.1007/s00343-020-0124-4

Steady increase in water clarity in Jiaozhou Bay in the Yellow Sea from 2000 to 2018: Observations from MODIS*

Ziyao YIN[1, 2], Junsheng LI[1, 2, **], Jue HUANG[3], Shenglei WANG[4], Fangfang ZHANG[1], Bing ZHANG[1, 2]

[1] *Key Laboratory of Digital Earth Science*, *Aerospace Information Research Institute*, *Chinese Academy of Sciences*, *Beijing 100094*, *China*

[2] *University of Chinese Academy of Sciences*, *Beijing 100049*, *China*

[3] *College of Geomatics*, *Shandong University of Science and Technology*, *Qingdao 266590*, *China*

[4] *Institute of Remote Sensing and Geographic Information System*, *Peking University*, *Beijing 100871*, *China*

Received Mar. 27, 2020; accepted in principle May 25, 2020; accepted for publication Jul. 10, 2020

Abstract The Moderate Resolution Imaging Spectroradiometer (MODIS) surface reflectance data were used to analyze the temporal and spatial distribution characteristics of water clarity (Z_{sd}) in the Jiaozhou Bay, Qingdao, China, in the Yellow Sea from 2000 to 2018. Z_{sd} retrieval models were regionally optimized using in-situ data with coincident MODIS images, and then were used to retrieve the Z_{sd} products in Jiaozhou Bay from 2000–2018. The analysis of the Z_{sd} results suggests that the spatial distribution of relative Z_{sd} spatial characteristics in Jiaozhou Bay was stable, being higher Z_{sd} in the southeast and a lower Z_{sd} in the northwest. The annual mean Z_{sd} in Jiaozhou Bay showed a significant upward trend, with an annual increase of approximately 0.02 m. Water depth and wind speed were important factors affecting the spatial distribution and annual variation of Z_{sd} in Jiaozhou Bay, respectively.

Keyword: water clarity; Jiaozhou Bay; Moderate Resolution Imaging Spectroradiometer (MODIS); spatial distribution

1 INTRODUCTION

Water clarity (or water transparency) is an important parameter that indicates the degree of turbidity, a key ecological index that is indicative of the light transmission capacity of water (Lee et al., 2018; Shi et al., 2018). It also serves as a basic parameter in water quality investigations. Monitoring temporal and spatial changes in water clarity is of great importance to studies on water optical parameters, physical and chemical properties, water quality changes, and water eutrophication (Gong, 2012; Bukata, 2013; Yu et al., 2014). Water clarity is traditionally monitored using the Secchi disk method, which is also known as the Secchi disk depth (Z_{sd}, unit: m). The black-white Secchi disk with a diameter generally about 30 cm is gradually lowered into the water at the surface until it disappears out of the observer's sight. Here, the vertical distance between the observer's sight and water surface is the Z_{sd} of the water body. Although this method is simple to perform, the obtained data are discontinuous, the experiments are time-consuming and expensive, and real-time synchronization suffers from poor quality (Gong, 2012; Lee et al., 2018). However, remote sensing technology can acquire macroscopic, timely, accurate, and periodic data for a wide range of Z_{sd} distribution characteristics, especially in areas where access is difficult to monitor. Therefore, remote sensing technologies have gradually become an important and effective means to monitor water clarity (Chen et al., 2007; Gong, 2012; Bukata, 2013; Lee et al., 2018).

* Supported by the National Key Research and Development Program of China (No. 2017YFC0405804), the National Natural Science Foundation of China (Nos. 41971318, 41701402, 41901272), and the Science and Technology Service Network Initiative, Chinese Academy of Sciences (No. KFJ-STS-ZDTP-077)
** Corresponding author: lijs@radi.ac.cn

Over the past 30 years, numerous studies have shown that the Z_{sd} distribution in both open ocean and inland waters can be obtained from different types of remote sensing satellite data, including SeaWiFS, MODIS, MERIS, and Landsat TM/ETM+/OLI. At present, these studies have used remote sensing satellite data to retrieve Z_{sd} characteristics and proposed various remote sensing methods. One of these methods is a semi-analytical model based on physical theories, such as a model based on the classic underwater visibility theory (Duntley, 1960), a second based on the diffuse attenuation coefficient (K_d, /m) (Bukata et al., 1988; Kratzer et al., 2003; Aas et al., 2014; Alikas et al., 2015), and a third based on the remote sensing reflectance ($R_{rs}(\lambda)$), which corresponds to the spectral wavelengths from the visible domain (410–665 nm) (Lee et al., 2015, 2016). Finally, there is an empirical or semi-empirical model based on the use of band or band combinations, the band/band combination, or spectral coefficients, which include green band algorithms at approximately 550 nm (Binding et al., 2007), red band algorithms at approximately 645 nm (Shi et al., 2018), blue-red band ratio algorithms (Kratzer et al., 2008; Olmanson et al., 2008), spectral coefficient algorithms based on the surrounding baseline area and spectral curves in the 430- and 750-nm bands (Thiemann and Kaufmann, 2002), and algorithms based on the Forel-Ule index (FUI) and hue angle (α) (Van der Woerd and Wernand, 2015; Wang et al., 2015). Some Z_{sd} retrieval algorithms have been applied to analyze the temporal and spatial variations of water clarity in many areas (Barnes et al., 2013; Shang et al., 2016; Hou et al., 2017). Remote sensing technology plays an important role in the analysis of temporal and spatial variations of Z_{sd}, and it can also explore the causes for such changes.

Jiaozhou Bay is a semi-enclosed bay located in the southern coast of the Shandong Peninsula, China. It is the largest semi-enclosed bay of China, in Qingdao City, one of the biggest industrial cities in the northern China. With rapid coastal economic development, a large number of artificial buildings, such as aquaculture ponds, salt ponds, ports, wharves, and bridges, have gradually been built in the Jiaozhou Bay area, which has resulted in the gradual transformation of most of the coastline from natural to artificial areas (Zhang et al., 2015). In addition, Jiaozhou Bay has been eutrophicated over the last 30 years. (Jiao, 2001; Shen, 2001; Han et al., 2011). The Jiaozhou Bay Bridge, which was built in 2007, has also had a major impact on the hydrodynamic

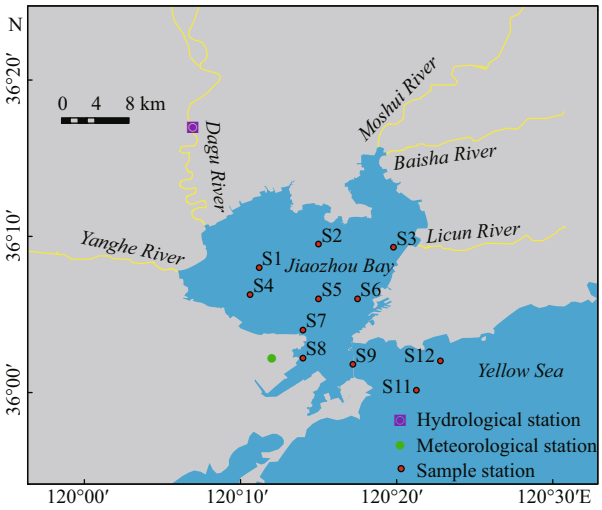

Fig.1 Locations of sampling, meteorological, and hydrological stations in Jiaozhou Bay

environment of Jiaozhou Bay. Collectively, Jiaozhou Bay is an ideal study site to investigate the natural and anthropogenic influences on the variation of water quality. Z_{sd} distribution characteristics will provide additional information regarding water mass analysis, stream identification, marine primary productivity, and regional oceanography for the waters that surrounding Jiaozhou Bay, as well as for environmental assessments and ecological protection planning. However, there is a lack of information on the temporal and spatial distribution of Z_{sd} in Jiaozhou Bay, and its natural and anthropogenic driving forces.

Based on MODIS data, we monitored the temporal and spatial changes in Z_{sd} in Jiaozhou Bay from 2000–2018 and analyzed its main influencing factors. First, we tested and optimized the Z_{sd} retrieval model suitable for Jiaozhou Bay and then produced the Z_{sd} product for Jiaozhou Bay from 2000–2018. In addition, we analyzed the influence that the environment (water depth), climate (wind speed, precipitation, and river discharge), and human activities have on the annual and spatial variations of Z_{sd} in Jiaozhou Bay.

2 DATA AND METHOD

2.1 Data

2.1.1 Study area

Jiaozhou Bay (36°06′N–36°25′N; 120°10′E–120°37′E; Fig.1) is located in Qingdao, Shandong Peninsula, China. The coastal administrative regions include districts of Shinan, Shibei, Licang, Chengyang, Laoshan, Jimo, Huangdao, and Jiaozhou.

Jiaozhou Bay covers an area of nearly 500 km^2 and is characterized by a complex underwater topography. The average water depth is approximately 7 m, with a maximum water depth of approximately 64 m (Song et al., 2015; Zhao et al., 2015). The main rivers flowing to Jiaozhou Bay include the Dagu, Moshui, Baisha, and Yanghe rivers. Due to the advancement of economic activities, and Qingdao City's recent population increase, these rivers have become discharge trenches for industrial and domestic waste waters (Shen, 2001; Liu et al., 2011).

2.1.2 In-situ data

The observed Z_{sd} data in Jiaozhou Bay were obtained from the Jiaozhou Bay Marine Ecosystem Research Station (http://jzw.qdio.cas.cn/). A total of 29 water samples from stations S1–S12 were collected on the following dates: December 11, 2008 (7 Z_{sd} measurements), July 15, 2009 (7 Z_{sd} measurements), December 17, 2010 (7 Z_{sd} measurements), August 19, 2013 (3 Z_{sd} measurements), and September 10, 2015 (5 Z_{sd} measurements) (Fig.1). The Z_{sd} values were measured using a standard black-white disk of 30 cm.

2.1.3 Remote sensing data

The remote sensing data selected in this study was derived from MODIS-Terra data, which was launched in 2000. Therefore, we can perform long-term time series analysis using this data, which is the case for previous studies that have successfully applied this data to analyze turbid offshore and inland waters (Feng et al., 2012; Li et al., 2017; Wang et al., 2018). The MODIS surface reflectance product (MOD09) provided 500-m spatial resolution data at seven bands across the visible, near-infrared, and short-wave infrared wavelengths. Five scenes of MOD09 images, which were concurrent with the in-situ data, were used to calibrate and validate the Z_{sd} estimation model. The calibrated and validated Z_{sd} estimation model was then applied to the 8-day composite MOD09 products, which are called MOD09A1 products. The reason why MOD09A1 was used in this paper is that it can provide data over a longer time range than MYD09A1. Also, it has been used for long-term and large-area water quality monitoring research as this dataset is well georeferenced, synthesized, and cloud marked (Feng et al., 2012; Wu et al., 2013; Li et al., 2016; Hou et al., 2017; Klein et al., 2017; Wang et al., 2018). The MOD09A1 data, which covered Jiaozhou Bay from 2000-2018, was obtained from the U.S. NASA Goddard Space Flight Center (GSFC, http://oceancolor.gsfc.nasa.gov/). The MOD09A1 data contains 868 good-quality scenes (spring: 209 scenes, summer: 209 scenes, autumn: 228 scenes, winter: 222 scenes) that were selected after visual examination and exclusion of scenes that were affected by clouds, sun glint, and thick aerosols.

2.1.4 Meteorological and hydrological data

We obtained daily average wind speed and precipitation data from 2000–2017 from the China Meteorological Data Network (http://data.cma.cn), which was collected from the nearest meteorological station (Qingdao Station) in Jiaozhou Bay. This was done in order to analyze the factors that affect the temporal and spatial variations in Z_{sd}. The daily average wind speed during the day of in-situ measurements was less than 4 m/s, and the water surface was relatively calm. Therefore, it can be considered that the value of Z_{sd} did not change considerably within hours of the difference between the in-situ measured data and the MODIS retrieved data. We also obtained monthly average river discharge data from the Nancun Hydrological Station in Dagu River from 2000–2013.

2.2 Method

To determine an appropriate Z_{sd} retrieval algorithm for Jiaozhou Bay, the MOD09A1 images first required preprocessing, followed by calibration and the testing of various retrieval methods based on satellite-ground synchronous data.

2.2.1 Data pre-processing

The MOD09A1 data required a series of pre-processing, including water-leaving reflectance correction and water body identification and extraction.

MODIS surface reflectance products (MOD09) were first atmospherically corrected for effects from atmospheric gases, aerosols, thin cirrus clouds, and for land adjacency effects (Vermote and Vermeulen, 1999). But the MOD09 data was still inadequate to monitor water quality parameters because of the effects of residual aerosol scattering, solar flares, and skylight reflection. In this study, a method was adopted to reduce noise in the MOD09 data and convert it into $R_{rs}(\lambda)$ by subtracting the near-infrared (NIR) minimum value from the shortwave infrared (SWIR) band and dividing by π (Wang et al., 2016). Previous studies have shown that this method easily and steadily yields good performance when

calculating $R_{rs}(\lambda)$ for different inland water bodies with exposure to different conditions (Wang et al., 2016, 2018).

Due to influences from changes in water volume, the water boundary, to a certain extent, is characterized by dynamic changes. Therefore, we used the modified histogram bimodal method (MHBM) to segment the water body (Zhang et al., 2018) based on the reflectance of the short wave infrared remote sensing data in the 1 640 nm band. In order to reduce the effect of adjacent land pixels (which have a higher reflectance) the coastline was extended seawards by two pixels (Feng and Hu, 2017).

2.2.2 Calibration and validation of Z_{sd} models

Out of the 29 measured Z_{sd} data samples, 20 were selected as the training samples to construct the model. The nine remaining samples were used as test samples to verify the model. Satellite products and field measurements have different temporal and spatial resolutions. It is necessary to determine a reasonable spatiotemporal window according to the spatial resolution of satellite products, as well as the spatiotemporal variation and uniformity of water bodies. Means of effective pixels in the spatial window and effective field measurements in the time window were taken as matching data pairs and incorporated into the validation data set. Several criteria were followed in obtaining matching pairs (Le et al., 2013; Feng et al., 2015). First, the time difference between field measurements and remote sensing images should be within ±3 h, and the wind speed during the day should be less than 4 m/s. Second, the water around the observation station should be uniform. Thus, a 3×3 pixel window centered on the measured site was selected. If the number of effective pixels, not including cloud and sun-glint, in the window exceeds five and the coefficient of variation (CV) of the effective pixels is less than 0.4, the average pixel value of the window is calculated as the final value.

To obtain the optimal model to retrieve the Z_{sd} values in Jiaozhou Bay based on the MODIS data, we used the 20 training samples to calibrate several commonly used Z_{sd} estimation models, including the red band algorithms (Shi et al., 2018), blue-red band ratio algorithms (Kratzer et al., 2008; Olmanson et al., 2008), green band algorithms (Binding et al., 2015), red-green band ratio algorithms (Duan et al., 2009; Ren et al., 2018), the Forel-Ule index (FUI), and the hue angle (α) algorithms (Van der Woerd and Wernand, 2015; Wang et al., 2015). The R^2 value for each model was calculated. Using the test samples, we then calculated the mean relative error (MRE) and correlation coefficient (r) of the measured and retrieved data (Table 1). MRE was defined as follow:

$$\mathrm{MRE}=\frac{1}{N}\sum_{i=1}^{n}\frac{\left|Y_i-X_i\right|}{X_i}\times 100\%, \tag{1}$$

where Y_i and X_i are the derived Z_{sd} and field measurements Z_{sd}, respectively. N is the number of matchups.

Out of these algorithms, the methods based on the FUI and α were the most complex. To obtain these two parameters, we used the Red, Green, Blue (RGB) conversion method to calculate X, Y, Z in the International Commission on Illumination (Commission Internationale de l'Eclairage, CIE) color system using the $R_{rs}(\lambda)$ of three visible bands (469, 555, and 645 nm) (CIE, 1931; Wang et al., 2015; Li et al., 2016).

$$\begin{aligned}X&=2.7689R_{rs}(645)+1.7517R_{rs}(555)+1.1302R_{rs}(469),\\ Y&=1.0000R_{rs}(645)+4.5707R_{rs}(555)+0.0601R_{rs}(469),\\ Z&=0.0000R_{rs}(645)+0.0565R_{rs}(555)+5.5934R_{rs}(469).\end{aligned} \tag{2}$$

The CIE chromaticity coordinates (x, y) were obtained by normalizing X, Y, and Z to 0 and 1 as follows (CIE, 1931; Wang et al., 2015).

$$x=\frac{X}{X+Y+Z},\ y=\frac{Y}{X+Y+Z}. \tag{3}$$

The hue angle α were calculated by the new definition in Wang et al. (2018), which has positive range from 0 to 2π from the downward x axis clockwise:

$$\alpha=\arctan(x-1/3, y-1/3)+\pi. \tag{4}$$

To eliminate systematic deviation caused by hyperspectral $R_{rs}(\lambda)$ and the equivalent MODIS bands, the corrected hue angle α was obtained using the method reported in Wang et al. (2018), which was based on the methods proposed in Van der Woerd and Wernand (2015), but with the new definition of α start axis and direction. Finally, the FUI was calculated using the lookup table (Table 2) based on the corrected hue angle α, which is transformed from the look-up-table in Novoa et al. (2013) with the new definition of α start axis and direction.

By comparison, we observed that the Z_{sd} retrieval model based on α had the highest accuracy, with a model MRE of 36%, as well as elevated model and test R^2 values compared with the other models. This indicates that, compared with other commonly used

Table 1 Calibration and evaluation of the various tested Z_{sd} retrieval models for Jiaozhou Bay

Band or spectral index	Optimized model	MRE (%)	Model R^2	r of measured andretrieval data
$X_1=R_{rs}$(blue)/R_{rs}(red) $X_2=R_{rs}$(red)	$Z_{sd}=1.99+0.052X_1+9.173X_2$	67	0.03	-0.69
$X=R_{rs}$(green)	$Z_{sd}=1.3X–0.148$	48	0.01	0.70
$X=R_{rs}$(blue)/R_{rs}(red)	$Z_{sd}=–0.126X^2+1.678X+0.668$	53	0.33	0.26
$X=\ln(R_{rs}(red)/R_{rs}(green))$	$Z_{sd}=1.097X^3+6.306X^2+6.888X+4.01$	73	0.10	0.24
$X=R_{rs}$(red)/R_{rs}(green)	$Z_{sd}=1.974+0.731X$	62	0.02	0.003
$X=R_{rs}$(red)	$Z_{sd}= 479.035X^2–41.004X+1.269$	66	0.19	0.25
X=FUI	$Z_{sd}=0.274+16.352/X$	41	0.59	0.69
$X=\alpha$	$Z_{sd}=5.524–0.019X$	36	0.61	0.72

The table quotes the coefficient of determination (R^2) for each regression model calibrated and tested against in-situ data (n=20, see example Fig.2a), as well as the mean relative error (MRE) of each model tested on an independent data set (n=9), and the correlation coefficient r for the test (see example in Fig.2b).

Table 2 21 levels of FUI and the corresponding hue angle α values in the Forel-Ule scales

FUI	1	2	3	4	5	6	7	8	9	10	11
α	40.5	45.2	52.9	67.2	91.3	122.6	151.5	170.5	181.5	191.8	199.0
FUI	12	13	14	15	16	17	18	19	20	21	
α	205.1	210.6	216.6	222.1	227.6	232.8	237.4	241.8	245.6	249.0	

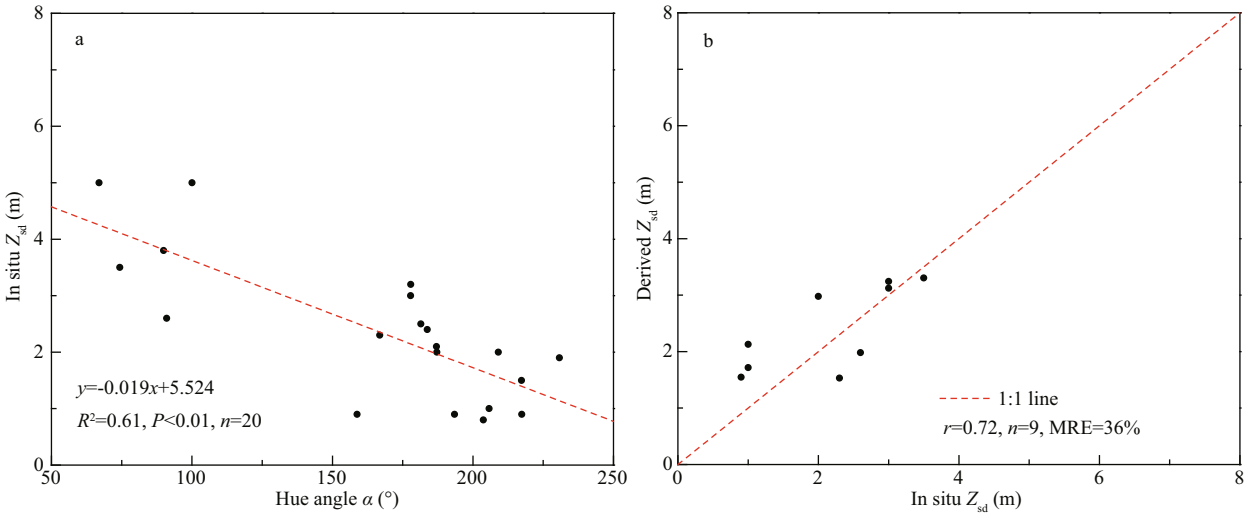

Fig.2 Calibration (a) and validation (b) of the proposed model to estimate Z_{sd} in Jiaozhou Bay

Z_{sd} retrieval models, the model based on α had higher retrieval accuracy and was more suitable for Z_{sd} retrieval in the Jiaozhou Bay area. Z_{sd} showed a linear decrease with increasing hue angle α (Fig.2a). There was a negative correlation between Z_{sd} and α, with a model R^2 of 0.61. Equation 1 defines the developed model:

$$Z_{sd}=5.524–0.019\alpha. \quad (5)$$

The paired data were characterized by a significant correlation that was predominantly located near the 1:1 line (Fig.2b; R^2=0.518), which demonstrated that the model was effective and can be used to derive the Z_{sd} in Jiaozhou Bay. Therefore, the model based on α was chosen for the derivation and the further analysis of the Z_{sd} in Jiaozhou Bay.

3 RESULT

Based on the MOD09A1 products that cover Jiaozhou Bay from 2000–2018, the long-term Z_{sd} product for Jiaozhou Bay was derived using the established retrieval model based on α. Based on this product, we analyzed the Z_{sd} temporal and spatial distribution and variation characteristics in Jiaozhou Bay.

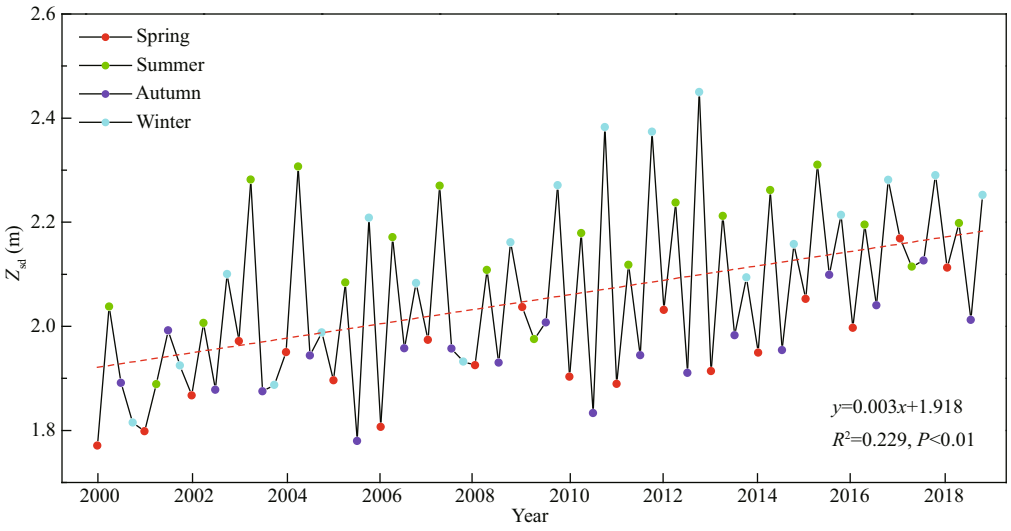

Fig.3 Mean MODIS seasonal time series and Z_{sd} linear regression line from 2000–2018

3.1 Temporal variation in Z_{sd}

3.1.1 Seasonal variation

The Z_{sd} in Jiaozhou Bay varied significantly, ranging from a minimum value of 1.8 m in the spring of 2000 to a maximum value of 2.5 m in the winter of 2012, with a mean long-term Z_{sd} mean value of 2.1 m (Fig.3). Over the past 19 years, the Z_{sd} of Jiaozhou Bay has been slowly increasing, but there were no obvious seasonal variations. The Z_{sd} in summer (June–August) and winter (December–February) were higher than that in spring (March–May) and autumn (September–November), but the seasonal variations were not stable from year to year.

3.1.2 Inter-annual variation

The mean annual Z_{sd} was lowest in 2000, which was 1.8 m, and the highest in 2016, which was 2.2 m (Figs.4 & 5). The mean annual Z_{sd} in Jiaozhou Bay from 2000–2018 showed a significant upward trend (R^2=0.78, P<0.01), with a mean annual increase of 0.02 m. However, there was a sharp decline in the Z_{sd} in 2008 that deviated from the inter-annual trend line (Fig.5). Annual Z_{sd} in Jiaozhou Bay was inversely correlated with wind speed (R^2=0.65, P<0.01).

3.2 Spatial distribution characterization of Z_{sd}

The MODIS derived Z_{sd} data from 2000–2018 were averaged to calculate the Z_{sd} distribution in Jiaozhou Bay (Fig.6a). Z_{sd} in Jiaozhou Bay gradually increased from the northwest to the southeast. The Z_{sd} was highest in the southeastern region near the open sea area while the lowest value was in the northwest coastal estuary. The Z_{sd} spatial distribution in Jiaozhou Bay was consistent for each year (Fig.4).

The spatial distribution of CV was also calculated from the MODIS derived Z_{sd} values from 2000–2018 (Fig.6b). The CV increased from the inside to the outside of Jiaozhou Bay, ranging from 0 to 82%, with an average of 27%. This demonstrated that there was a certain Z_{sd} spatial variation. The lowest Z_{sd} values and the largest CV values were found in the coastal areas of Jiaozhou Bay that are connected to inland regions by several rivers and streams, while the lowest values were observed in the middle of Jiaozhou Bay. This indicates that Z_{sd} variations in the coastal areas of Jiaozhou Bay which are strongly influenced by humans activities and coastal runoff.

4 DISCUSSION

4.1 Driving factor

The above results demonstrate that Z_{sd} values in Jiaozhou Bay had clear temporal and spatial variations. We attempted to analyze the influence that the topography (water depth), hydrological (wind speed, precipitation, and river discharge), and human activities have on the annual, seasonal, and spatial variations of Z_{sd} in Jiaozhou Bay.

4.1.1 Water depth

Xue et al. (2015) reported that water depth and runoff had the greatest impact on the Z_{sd} distribution in Chinese offshore waters. Based on the water depth distribution map of Jiaozhou Bay reported in Ye et al. (2009), we divided it into five levels from low to high

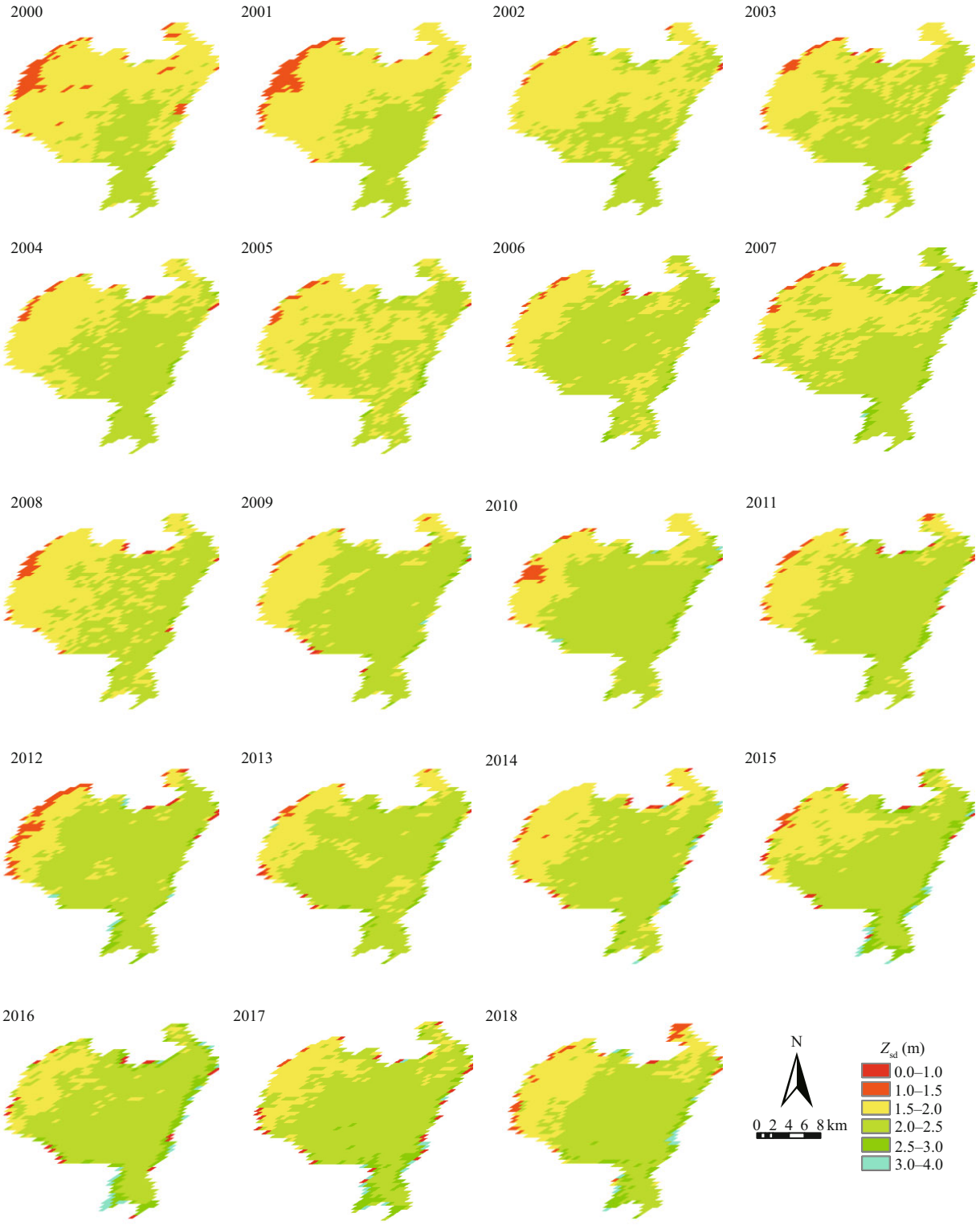

Fig.4 MODIS-derived mean annual Z_{sd} in Jiaozhou Bay from 2000 to 2018

The Secchi depth has steadily increased over the observation period, indicating an improvement in water quality.

(Fig.6a) and superimposed it with the mean Z_{sd} from 2000–2018 to calculate the mean Z_{sd} of each water depth level area.

Z_{sd} in Jiaozhou Bay noticeably increased with increasing water depths (Fig.6a). The mean Z_{sd} of the five regions in Fig.6a was 1.6, 1.7, 1.9, 2.0, and 2.1 m,

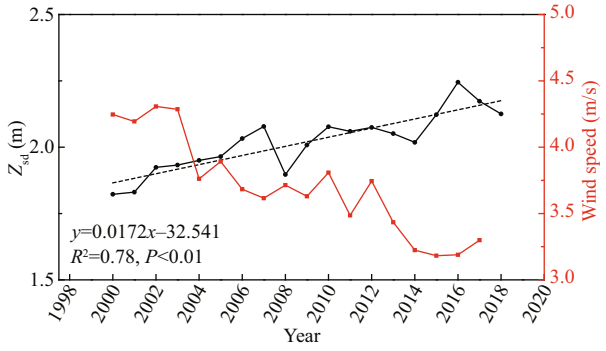

Fig.5 Mean annual MODIS-derived Z_{sd} from 2000–2018 and mean annual wind speeds measured at Qingdao meteorological station from 2000–2017

Z_{sd} was inversely correlated with wind speed (R^2=0.65, P<0.01).

with low and high Z_{sd} values at nearshore and offshore locations, respectively, which indicates that water depth is an important factor that affects the Z_{sd} spatial distribution in Jiaozhou Bay. Shallow depths are usually found in near-coastal areas while deeper waters are found in the inner bay. Coastal runoff transports a large amount of suspended sediment to the sea. In shallow coastal areas bottom sediments are easily re-suspended when exposed to waves and currents, which increases the concentration of suspended solids in the water column. The water depth mainly affects the spatial distribution of Z_{sd} but seems to have little effect on the temporal variations in Z_{sd} (Figs.4 & 6).

4.1.2 Wind speed

The inter-annual variations in the Z_{sd} values had a negative correlation with wind speed (R^2=0.649, P<0.01; Fig.7a) indicating that lower wind speeds corresponded to higher Z_{sd} values. This is possibly due to the fact that increased wind speeds in Jiaozhou Bay facilitate resuspension and transportation of sediments deposited on the seabed, thus leading lower Z_{sd} values (Booth et al., 2000; Gao et al., 2017; Feng et al., 2019). Therefore, the significant inter-annual Z_{sd} fluctuations in Jiaozhou Bay may also be due to inter-annual variations in wind or sand resuspension. Based on the annual Z_{sd} variations in Jiaozhou Bay (Fig.5), Z_{sd} has been significantly higher since 2015 compared with the years before 2015, which is due to lower wind speeds between 2015 and 2018 compared with previous years. The results clearly suggest that wind speed is an important factor affecting the inter-annual Z_{sd} variations in Jiaozhou Bay.

4.1.3 Precipitation and river discharge

Precipitation data were averaged with respect to year and compared with the mean annual Z_{sd} (Fig.7b). We observed that the correlation between these parameters was not significant for the annual time scales (R^2=0.044, P=0.40). The analysis showed that precipitation has a relatively small effect on the Z_{sd} in Jiaozhou Bay and thus is not a key factor influencing inter-annual Z_{sd} variations in Jiaozhou Bay. This is normal, because precipitation mainly affects the short-term change in Z_{sd}, but not the long-term change such as inter-annual change (Song et al., 2015).

For the relationship between river discharge and Z_{sd} in Jiaozhou Bay, we must consider the 16 rivers that flow into Jiaozhou Bay, which include the Dagu, Moshui, Baisha, Yanghe, and Licun rivers. Out of these rivers, Dagu River has the largest catchment

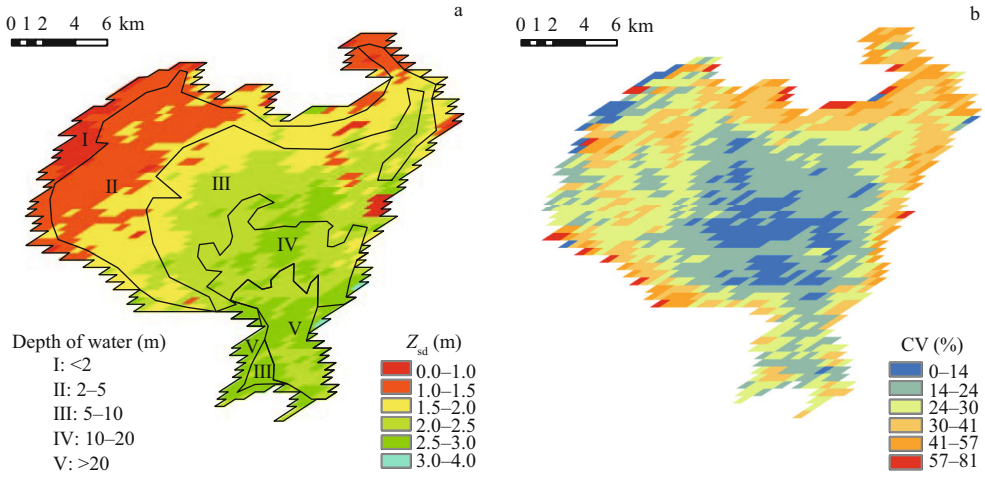

Fig.6 Spatial distribution of Z_{sd} in Jiaozhou bay based on the average Z_{sd} estimates from all MODIS data collected during 2000–2018 (a) and the spatial distribution of the mean CV in Jiaozhou bay based on all Z_{sd} estimates from the MODIS data collected during 2000–2018 (b)

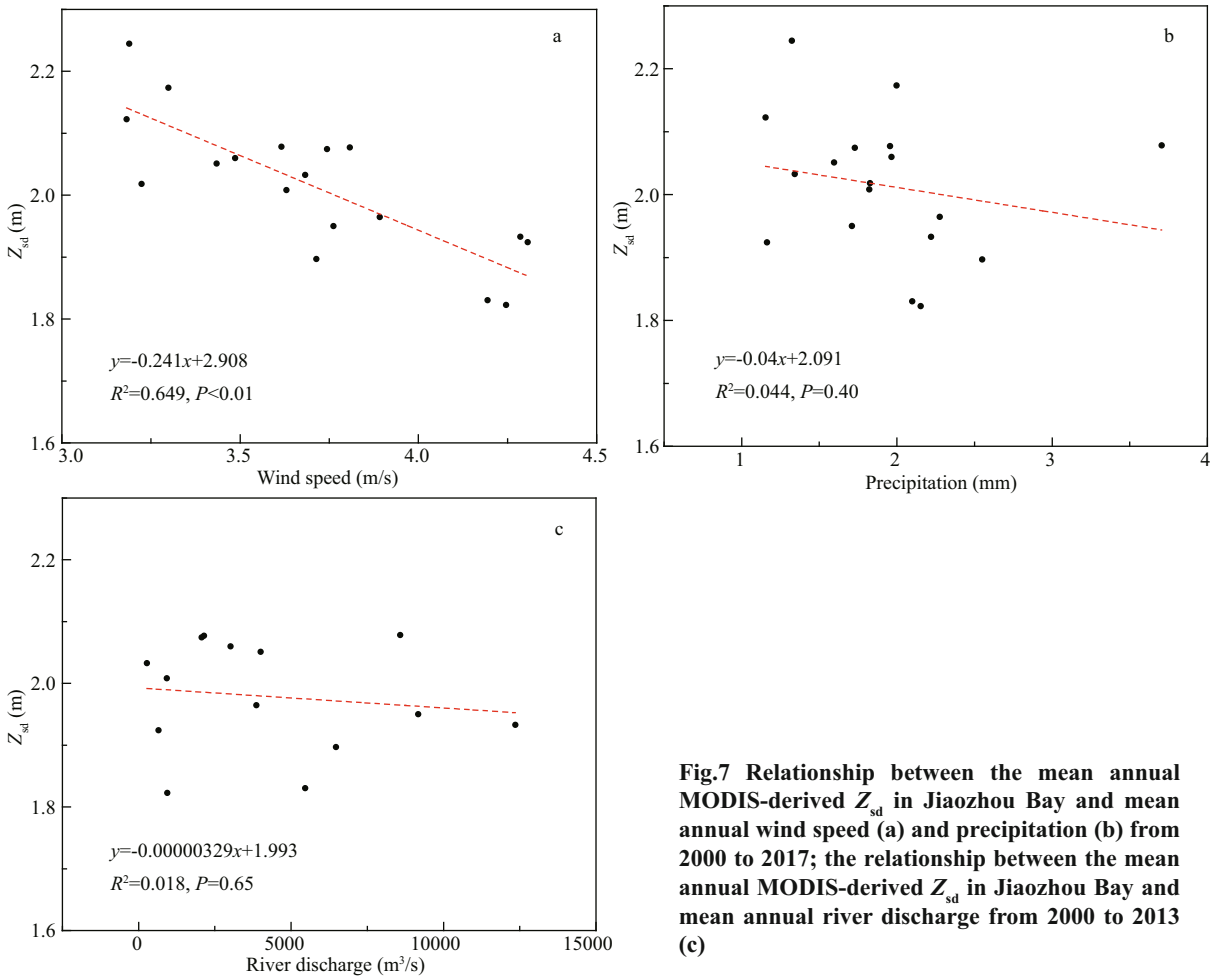

Fig.7 Relationship between the mean annual MODIS-derived Z_{sd} in Jiaozhou Bay and mean annual wind speed (a) and precipitation (b) from 2000 to 2017; the relationship between the mean annual MODIS-derived Z_{sd} in Jiaozhou Bay and mean annual river discharge from 2000 to 2013 (c)

area, which occupies 82% of the total catchment area of the Jiaozhou Bay river system (Jiang and Wang, 2013). Average monthly river discharge from Nancun Hydrological Station, which exists for 2000–2013, was used to analyze the relationship. Nancun Hydrological Station is located in the middle and lower reaches of the main stem of the Dagu River. Nancun is the closest station to the lower reaches of the Dagu River, with long-term river discharge data, and is representative of the overall flow characteristics in the basin. Dagu River is a river that is mostly fed by precipitation, and thus is subject to strong fluctuations in water levels. The flood season for the Dagu River occurs in the summer.

Using the same method to analyze the relationship between the mean annual river discharge and Z_{sd} (Fig.7c), we found that there was no clear correlation between these parameters (R^2=0.018, P=0.65). This suggests that the influence that river discharge has on Z_{sd} in Jiaozhou Bay is not significant, as well as the fact that river discharge is not the main factor that affects annual variations in Jiaozhou Bay.

4.1.4 Human activity

Human activity has an important impact on the temporal and spatial Z_{sd} variations in Jiaozhou Bay. Z_{sd} can also reflect changes, to a certain extent, in ecological environments in Jiaozhou Bay, which is of great significance to urban development planning. Z_{sd} variations in the bay were mainly concentrated in coastal areas, whereas variations in the center of the bay were relatively small. This is likely due to the fact that coastal areas are more directly affected by anthropogenic factors, such as industrial pollution.

During the construction of the Jiaozhou Bay Bridge (2007–2010), Z_{sd} values in the Jiaozhou Bay decreased compared with those of previous years, reaching their lowest level in 2008, which was only 1.9 m. After the bridge was completed and opened to traffic, the Z_{sd} values displayed an upward trend. The mean Z_{sd} during bridge construction was 2.0 m, while that after bridge construction was 2.1 m, mainly due to the construction of Jiaozhou Bay Bridge, which officially began in 2007 and was completed the following year.

A large number of operations associated with bridge foundations churned the water, which resulted in a sharp decline in the mean annual Z_{sd} value in 2008. With the completion of the bridge, the Z_{sd} value in the Jiaozhou Bay area began to gradually rise beginning in 2009. Relevant studies have shown that the construction of the Jiaozhou Bay Bridge has affected the hydrodynamic conditions in Jiaozhou Bay (Zhang et al., 2015) and further affected the spatial and temporal distribution of sea ice in Jiaozhou Bay in the winter (Huang et al., 2019). We infer that the changes in the hydrodynamic conditions in Jiaozhou Bay caused by the construction of the sea-crossing bridge, as well as operations, such as bridge piling, will cause sediment resuspension, which also has an impact on the Z_{sd} distribution. Based on our analyses, it is clear that human activity rapidly changes the Z_{sd}, such that human activity has an important impact on short-term annual Z_{sd} variations in Jiaozhou Bay.

4.1.5 Summary of driving factor

The spatial Z_{sd} distribution in Jiaozhou Bay displayed a trend of elevated values in the southeast and lower values in the northwest. The water depth distribution had a trend of high values in the southeast and decreased values in the northwest. In contrast, the northwestern region of Jiaozhou Bay is contiguous with inland areas, and is significantly influenced by human activity, such as industrial pollution, while the southeastern areas connect with the sea, such that the water is relatively clean. In addition, rivers along the coast, such as the Dagu, Moshui, and Baisha rivers, are mainly located in the northwestern and northern parts of Jiaozhou Bay. Therefore, when it rains, rivers have a greater effect on the northwest region, where changes in the river discharge contribute to changes in Z_{sd}. Compared with wind, rainfall and river discharge, it was found that wind speed had a greater impact on the inter-annual Z_{sd} variations in Jiaozhou Bay. Meanwhile, we explored the factors governing seasonal Z_{sd} variations. We calculated the relationships between the seasonal average wind speed, precipitation, and river discharge, and the seasonal average Z_{sd}, and found that the correlations are not strong (R^2=0.3, 0.018, and 0.004, respectively). Therefore, there are possibly other factors on the seasonal scale that result in unstable seasonal Z_{sd} variations. In addition, human activity has a significant influence on short-term annual variations in $Z_{sd.}$

4.2 Uncertainty and future application

The biggest challenge associated with the long-term-scale Z_{sd} retrieval model lies in its application to regional and seasonal scales, especially the stability of retrieval model in turbid waters. The commonly used quasi-analytical algorithm (QAA) based Z_{sd} retrieval model requires R_{rs} products (Lee et al., 2002), but because of the highly turbidity of Jiaozhou Bay, there is no available R_{rs} products. Therefore, only the surface reflectance product MOD09A1 can be used, but MOD09A1 only has 469, 555, 645, and 859 available bands, so QAA algorithm cannot be used. Therefore, other empirical or semi-empirical methods should be used. The theoretical basis for Z_{sd} retrieval using the hue angle α, is that water with different Z_{sd} values exhibiting different hues, where α can more accurately capture this change in information. Compared with other commonly used models, we observed that the model based on the hue angle had a higher accuracy with respect to Z_{sd} retrieval in Jiaozhou Bay. Therefore, a regional model suitable for the inversion of Z_{sd} in Jiaozhou Bay was proposed based on α.

Some studies have shown that there is good correlation between water color and Z_{sd} (Novoa et al., 2013; Van der Woerd and Wernand, 2015; Li et al., 2016; Wang et al., 2018). However, there are some limitations in the method of Z_{sd} based on FUI or α. The color of water is mainly determined by the total absorption spectrum of suspended matter, chlorophyll *a*, colored dissolved organic matter (CDOM), and pure water. When the optical properties of water are dominated by suspended matter, CDOM, or pure water, it is not easy to have the same color corresponding to different Z_{sd} values. However, when algae blooms occur, phytoplankton dominates the total absorption spectrum of the water, such that the color of the water does not change monotonously with the wavelength and the same color may correspond to different Z_{sd} values. Fortunately, for Jiaozhou Bay, which has no large-scale and long-term water bloom and whose absorption spectrum is dominated by suspended matter, the same water color does not correspond to different Z_{sd}. The atmospheric correction effect for remote sensing images is another challenge to water quality parameter retrieval. In this study, we adopted a correction method using the water-leaving reflectance based on the MODIS surface reflectance product, which essentially meets the retrieval requirements for the Jiaozhou Bay water-

leaving reflectance. Furthermore, several previous and related studies have indicated that α was less sensitive to observation conditions and aerosol types (Wang et al., 2018; Pitarch et al., 2019). In addition, the α value used in this model was derived from the corrected synchronous MODIS surface reflectance products, rather than the measured water-leaving reflectance, which could further reduce the impact that the atmosphere has on the retrieval results. Therefore, the Z_{sd} retrieval model using the MODIS hue angle α, can largely avoid the uncertainty associated with atmospheric correction.

Note that the accuracy of the measured Z_{sd} data may affect the model, especially in water characterized by high Z_{sd} values. The Z_{sd} measurements are vulnerable to wind speed, wave, and even ship navigation, which may lead to associated uncertainties. Therefore, high-precision data measurements will reduce model uncertainty. More measured data can further improve the Z_{sd} retrieval model. At the same time, the satellite transit time may be different from the measurement time (e.g., more than 3 h), which will also lead to certain errors in the Z_{sd} retrieval results (Feng et al., 2012).

Due to the complex water environment in Jiaozhou Bay, it is difficult to accurately obtain the characteristic changes in Z_{sd} using traditional field surveys. In this study, for the first time through the analysis of Z_{sd} MOD09A1 images in Jiaozhou Bay from the past 19 years, we were able to decipher the significant temporal and spatial changes in Z_{sd} in Jiaozhou Bay and its driving factors. Although the MODIS data is characterized by strong stability and the advantages of a global data product service, its spatial resolution is not sufficient to monitor small bodies of water. With the atmospheric correction for high spatial and spectral resolution remote sensing data, such as Landsat-8 OLI and the production of water products, the algorithm established in this study can be used with new sensor images to cover more water bodies, which can provide new possibilities and challenges when evaluating Z_{sd} changes in Jiaozhou Bay, as well as providing certain theoretical support to environmental assessments and ecological protection decision-making for the relevant governmental departments.

5 CONCLUSION

In this study, using an eight-day composite MODIS-Terra surface reflectance product (MOD09A1), we established a model to derive the Z_{sd} in Jiaozhou Bay using the CIE color space parameter of hue angle α. Using this model, we obtained the Z_{sd} products in Jiaozhou Bay from 2000 to 2018. We investigated the temporal and spatial distribution characteristics of the Z_{sd} in Jiaozhou Bay, as well as an analysis of its main influencing factors. The main conclusions of this study are as follows:

(1) The mean inter-annual Z_{sd} in Jiaozhou Bay from 2000–2018 ranged from 1.8 m to 2.5 m, with a mean value of 2.1 m. The variations in Z_{sd} with time showed an upward trend, with a mean annual increase of 0.02 m. Comparing wind, precipitation, river discharge, and other factors, we found that wind speed has a greater impact on Z_{sd}.

(2) The spatial distribution of Z_{sd} in Jiaozhou Bay was stable, showing high values in the southeast and low values in the northwest, where variations in Z_{sd} in coastal areas were much larger than those in the inner bay. Water depth was an important factor that caused the spatial distribution of Z_{sd} in Jiaozhou Bay. Deeper waters yield higher Secchi depths whilst more shallow areas are more influenced by resuspension of bottom sediments.

(3) Human activity has also caused changes in Z_{sd} to a certain extent, where human activity, such as the large-scale construction of artificial facilities, has an impact on the short-term annual variations in Z_{sd}.

This study shows that the Z_{sd} retrieval model based on hue angle α can be applied to turbid water. Although we only selected Jiaozhou Bay to test this model, we suggest that this method can be extended to other water bodies with similar optical characteristics and ranges in Secchi depth, such as Liaodong Bay, Bohai Bay, and Laizhou Bay to explore their Z_{sd} distributions. This study also shows that this method is a support tool for environmental managers to improve decision-making and governmental policies in Jiaozhou Bay.

6 DATA AVAILABILITY STATEMENT

The data of this study are available from the Jiaozhou Bay Marine Ecosystem Research Station but restrictions may apply due to the availability of some of the data that were used under license for this study, and thus, they are not publicly available. The data are however available from the authors upon reasonable request and with permission from the Jiaozhou Bay Marine Ecosystem Research Station.

7 ACKNOWLEDGMENT

The authors would like to thank NASA GSFC for providing MODIS data, and we are also grateful to

Jiaozhou Bay Marine Ecosystem Research Station for providing in-situ Z_{sd} data.

References

Aas E, Høkedal J, Sørensen K. 2014. Secchi depth in the Oslofjord-Skagerrak area: theory, experiments and relationships to other quantities. *Ocean Science*, **10**(2): 177-199, https://doi.org/10.5194/os-10-177-2014.

Alikas K, Kratzer S, Reinart A, Kauer T, Paavel B. 2015. Robust remote sensing algorithms to derive the diffuse attenuation coefficient for lakes and coastal waters. *Limnology and Oceanography*: *Methods*, **13**(8): 402-415, https://doi.org/10.1002/lom3.10033.

Barnes B B, Hu C M, Schaeffer B A, Lee Z P, Palandro D A, Lehrter J C. 2013. MODIS-derived spatiotemporal water clarity patterns in optically shallow Florida Keys waters: a new approach to remove bottom contamination. *Remote Sensing of Environment*, **134**: 377-391, https://doi.org/10.1016/j.rse.2013.03.016.

Binding C E, Greenberg T A, Watson S B, Rastin S, Gould J. 2015. Long term water clarity changes in North America's great lakes from multi-sensor satellite observations. *Limnology and Oceanography*, **60**(6): 1 976-1 995, https://doi.org/10.1002/lno.10146.

Binding C E, Jerome J H, Bukata R P, Booty W G. 2007. Trends in water clarity of the Lower Great Lakes from remotely sensed aquatic color. *Journal of Great Lakes Research*, **33**(4): 828-841, https://doi.org/10.3394/0380-1330(2007)33[828:TIWCOT]2.0.CO;2.

Booth J G, Miller R L, McKee B A, Leathers R A. 2000. Wind-induced bottom sediment resuspension in a microtidal coastal environment. *Continental Shelf Research*, **20**(7): 785-806, https://doi.org/10.1016/S0278-4343(00)00002-9.

Bukata R P, Jerome J H, Bruton J E. 1988. Relationships among Secchi disk depth, beam attenuation coefficient, and irradiance attenuation coefficient for Great Lakes waters. *Journal of Great Lakes Research*, **14**(3): 347-355, https://doi.org/10.1016/S0380-1330(88)71564-6.

Bukata R P. 2013. Retrospection and introspection on remote sensing of inland water quality: "Like Déjà Vu All Over Again". *Journal of Great Lakes Research*, **39 Suppl 1**: 2-5, https://doi.org/10.1016/j.jglr.2013.04.001.

Chen Z Q, Muller-Karger F E, Hu C M. 2007. Remote sensing of water clarity in Tampa Bay. *Remote Sensing of Environment*, **109**(2): 249-259, https://doi.org/10.1016/j.rse.2007.01.002.

CIE. 1931. Commission Internationale de l'Eclairage Proceedings. Cambridge Univ. Press, London, England. p.19-29.

Duan H T, Ma R H, Zhang Y Z, Zhang B. 2009. Remote-sensing assessment of regional inland lake water clarity in Northeast China. *Limnology*, **10**(2): 135-141, https://doi.org/10.1007/s10201-009-0263-y.

Duntley S Q. 1960. The visibility of submerged objects. *Scripps Institution of Oceanography*. p.16-21, https://escholarship.org/uc/item/2mz4d121.

Feng L, Hou X J, Zheng Y. 2019. Monitoring and understanding the water transparency changes of fifty large lakes on the Yangtze plain based on long-term MODIS observations. *Remote Sensing of Environment*, **221**: 675-686, https://doi.org/10.1016/j.rse.2018.12.007.

Feng L, Hu C M, Chen X L, Tian L Q, Chen L Q. 2012. Human induced turbidity changes in Poyang Lake between 2000 and 2010: observations from MODIS. *Journal of Geophysical Research Oceans*, **117**(C7): C07006, https://doi.org/10.1029/2011JC007864.

Feng L, Hu C M, Han X X, Chen X L, Lin Q. 2015. Long-term distribution patterns of chlorophyll-*a* concentration in China's largest freshwater lake: MERIS full-resolution observations with a practical approach. *Remote Sensing*, **7**(1): 275-299, https://doi.org/10.3390/rs70100275.

Feng L, Hu C M. 2017. Land adjacency effects on MODIS a qua top-of-atmosphere radiance in the shortwave infrared: statistical assessment and correction. *Journal of Geophysical Research*: *Oceans*, **122**(6): 4 802-4 818, https://doi.org/10.1002/2017JC012874.

Gao L, Yao H Y, Zhang M M, Ju L, Cao J. 2017. Temporal and spatial variation of seawater transparency and its relationship with environmental factors in Qingdao coastal area. *Journal of Marine Sciences*, **35**(3): 79-84, https://doi.org/10.3969/j.issn.1001-909X.2017.03.009. (in Chinese)

Gong P. 2012. Remote sensing of environmental change over china: a review. *Chinese Science Bulletin*, **57**(22): 2 793-2 801, https://doi.org/10.1007/s11434-012-5268-y.

Han H Y, Li K Q, Wang X L, Shi X Y, Qiao X D, Liu J. 2011. Environmental capacity of nitrogen and phosphorus pollutions in Jiaozhou Bay, China: modeling and assessing. *Marine Pollution Bulletin*, **63**(5-12): 262-266, https://doi.org/10.1016/j.marpolbul.2010.12.017.

Hou X J, Feng L, Duan H T, Chen X L, Sun D Y, Shi K. 2017. Fifteen-year monitoring of the turbidity dynamics in large lakes and reservoirs in the middle and lower basin of the Yangtze River, China. *Remote Sensing of Environment*, **190**: 107-121, https://doi.org/10.1016/j.rse.2016.12.006.

Huang J, Guo L J, Jiang T, Zhu H C. 2019. Three decades of sea-ice variability in Jiaozhou Bay revealed by Landsat observations. *Journal of Ocean University of China*, **18**(2): 349-357, https://doi.org/10.1007/s11802-019-3730-z.

Jiang D J, Wang X L. 2013. Variation of runoff volume in the Dagu River basin in the Jiaodong Peninsula. *Arid Zone Research*, **30**(6): 965-972. (in Chinese)

Jiao N Z. 2001. Ecological Processes and Sustainable Development of Typical Coastal Water Ecosystems in China. Science Press, Beijing, China. p.241-253. (in Chinese)

Klein I, Gessner U, Dietz A J, Kuenzer C. 2017. Global WaterPack—A 250 m resolution dataset revealing the daily dynamics of global inland water bodies. *Remote Sensing of Environment*, **198**: 345-362, https://doi.org/10.1016/j.rse.2017.06.045.

Kratzer S, Brockmann C, Moore G. 2008. Using MERIS full

resolution data to monitor coastal waters—a case study from Himmerfjärden, a fjord-like bay in the Northwestern Baltic Sea. *Remote Sensing of Environment*, **112**(5): 2 284-2 300, https://doi.org/10.1016/j.rse.2007.10.006.

Kratzer S, Håkansson B, Sahlin C. 2003. Assessing Secchi and photic zone depth in the Baltic Sea from satellite data. *AMBIO*: *A Journal of the Human Environment*, **32**(8): 577-585, https://doi.org/10.1579/0044-7447-32.8.577.

Le C F, Hu C M, Cannizzaro J, English D, Muller-Karger F, Lee Z P. 2013. Evaluation of chlorophyll-a remote sensing algorithms for an optically complex estuary. *Remote Sensing of Environment*, **129**: 75-89, https://doi.org/10.1016/j.rse.2012.11.001.

Lee Z P, Arnone R, Boyce D, Franz B, Greb S, Hu C M, Lavender S, Lewis M R, Schaeffer B, Shang S L, Wang M H, Wernand M, Wilson C. 2018. Global water clarity: continuing a century-long monitoring. *EOS*, **99**, https://doi.org/10.1029/2018EO097251.

Lee Z P, Carder K, Arnone R A. 2002. Deriving inherent optical properties from water color: a multiband quasi-analytical algorithm for optically deep waters. *Applied Optics*, **41**(27): 5 755-5 772, https://doi.org/10.1364/AO.41.005755.

Lee Z P, Shang S L, Hu C M, Du K P, Weidemann A, Hou W L, Lin J F, Lin G. 2015. Secchi disk depth: a new theory and mechanistic model for underwater visibility. *Remote Sensing of Environment*, **169**: 139-149, https://doi.org/10.1016/j.rse.2015.08.002.

Lee Z P, Shang S L, Qi L, Yan J, Lin G. 2016. A semi-analytical scheme to estimate Secchi-disk depth from Landsat-8 measurements. *Remote Sensing of Environment*, **177**: 101-106, https://doi.org/10.1016/j.rse.2016.02.033.

Li J S, Hu C M, Shen Q, Barnes B B, Murch B, Feng L, Zhang MW, Zhang B. 2017. Recovering low quality MODIS-terra data over highly turbid waters through noise reduction and regional vicarious calibration adjustment: a case study in Taihu Lake. *Remote Sensing of Environment*, **197**: 72-84, https://doi.org/10.1016/j.rse.2017.05.027.

Li J S, Wang S L, Wu Y H, Zhang B, Chen X L, Zhang F F, Shen Q, Peng D L, Tian L Q. 2016. MODIS observations of water color of the largest 10 lakes in China between 2000 and 2012. *International Journal of Digital Earth*, **9**(8): 788-805, https://doi.org/10.1080/17538947.2016.1139637.

Liu S M, Li R H, Zhang G L, Wang D R, Du J Z, Herbeck L S, Zhang J, Ren J L. 2011. The Impact of Anthropogenic activities on nutrient dynamics in the tropical Wenchanghe and Wenjiaohe estuary and lagoon system in east Hainan. *Marine Chemistry*, **125**(1-4): 49-68, https://doi.org/10.1016/j.marchem.2011.02.003.

Novoa S, Wernand M R, Van der Woerd H J. 2013. The Forel-Ule scale revisited spectrally: preparation protocol, transmission measurements and chromaticity. *Journal of the European Optical Society Rapid Publications*, **8**: 13057, https://doi.org/10.2971/jeos.2013.13057.

Olmanson L G, Bauer M E, Brezonik P L. 2008. A 20-year Landsat water clarity census of Minnesota's 10,000 lakes. *Remote Sensing of Environment*, **112**(11): 4 086-4 097, https://doi.org/10.1016/j.rse.2007.12.013.

Pitarch J, Van der Woerd H J, Brewin R J W, Zielinski O. 2019. Optical properties of Forel-Ule water types deduced from 15 years of global satellite ocean color observations. *Remote Sensing of Environment*, **231**: 111249, https://doi.org/10.1016/j.rse.2019.111249.

Ren J L, Zheng Z B, Li Y M, Lv G N, Wang Q, Lyu H, Huang C C, Liu G, Du C G, Mu M, Lei S H, Bi S. 2018. Remote observation of water clarity patterns in Three Gorges Reservoir and Dongting Lake of China and their probable linkage to the Three Gorges Dam based on Landsat 8 imagery. *Science of the Total Environmen*t, **625**: 1 554-1 566, https://doi.org/10.1016/j.scitotenv.2018.01.036.

Shang S L, Lee Z P, Shi L H, Lin G, Wei G M, Li X D. 2016. Changes in water clarity of the Bohai Sea: observations from MODIS. *Remote Sensing of Environment*, **186**: 22-31, https://doi.org/10.1016/j.rse.2016.08.020.

Shen Z L. 2001. Historical changes in nutrient structure and its Influences on phytoplantkon composition in Jiaozhou Bay. *Estuarine*, *Coastal and Shelf Science*, **52**(2): 211-224, https://doi.org/10.1006/ecss.2000.0736.

Shi K, Zhang Y L, Zhu G W, Qin B Q, Pan D L. 2018. Deteriorating water clarity in shallow waters: evidence from long term MODIS and in-situ observations. *International Journal of Applied Earth Observation and Geoinformation*, **68**: 287-297, https://doi.org/10.1016/j.jag.2017.12.015.

Song Z J, Gong L M, Chen Q, Gu Z K, Gao L, Huang H J. 2015. Influence on the Environment of the Coastal Area in Jiaozhou Bay of China. *Environmental Engineering and Management Journal*, **14**(8): 1 897-1 903, https://doi.org/10.30638/eemj.2015.202.

Thiemann S, Kaufmann H. 2002. Lake water quality monitoring using hyperspectral airborne data—a semiempirical multisensor and multitemporal approach for the Mecklenburg Lake District, Germany. *Remote Sensing of Environment*, **81**(2-3): 228-237, https://doi.org/10.1016/s0034-4257(01)00345-5.

Van der Woerd H J, Wernand M R. 2015. True colour classification of natural waters with medium-spectral resolution satellites: SeaWiFS, MODIS, MERIS and OLCI. *Sensors*, **15**(10): 25 663-25 680, https://doi.org/10.3390/s151025663.

Vermote E F, Vermeulen A. 1999. Atmospheric correction algorithm: spectral reflectances (MOD09). Algorithm theoretical background. National Aeronautics and Space Administration, p.18-39, http://modis.gsfc.nasa.gov/data/atbd/atbd_mod08.pdf.

Wang S L, Li J S, Shen Q, Zhang B, Zhang F F, Lu Z Y. 2015. MODIS-based radiometric color extraction and classification of inland water with the Forel-Ule scale: a case study of Lake Taihu. *IEEE Journal of Selected Topics in Applied Earth Observations and Remote Sensing*, **8**(2): 907-918, https://doi.org/10.1109/jstars.2014.2360564.

Wang S L, Li J S, Zhang B, Shen Q, Zhang F F, Lu Z Y. 2016. A simple correction method for the MODIS surface

reflectance product over typical inland waters in China. *International Journal of Remote Sensing*, **37**(24): 6 076-6 096, https://doi.org/10.1080/01431161.2016.1256508.

Wang S L, Li J S, Zhang B, Spyrakos E, Tyler A N, Shen Q, Zhang F F, Kuster T, Lehmann M K, Wu Y H, Peng D L. 2018. Trophic state assessment of global inland waters using a MODIS-derived Forel-Ule index. *Remote Sensing of Environment*, **217**: 444-460, https://doi.org/10.1016/j.rse.2018.08.026.

Wu G F, Cui L J, He J J, Duan H T, Fei T, Liu Y L. 2013. Comparison of MODIS-based models for retrieving suspended particulate matter concentrations in Poyang Lake, China. *International Journal of Applied Earth Observation and Geoinformation*, **24**: 63-72, https://doi.org/10.1016/j.jag.2013.03.001.

Xue Y H, Xiong X J, Liu Y Q. 2015. Distribution features and seasonal variability of the transparency in offshore waters of China. *Advances in Marine Science*, **33**(1): 38-44. (in Chinese)

Ye X M, Zheng Q A, Ji Y Q, Hua F, Lin Z S, Feng Y K. 2009. Water depth extraction from TM image in Jiaozhou Bay. *Hydrographic Surveying and Charting*, **29**(2): 12-15, 19, https://doi.org/10.3969/j.issn.1671-3044.2009.02.004. (in Chinese)

Yu D F, Xing Q G, Zhou B, Sun Y F, Zhou Y, Gai Y Y, Shi P. 2014. Retrieval of Secchi disk depth in Sishili Bay using the HJ-1B CCD image. *Marine Environmental Science*, **33**(4): 580-584. (in Chinese)

Zhang F F, Li J S, Zhang B, Shen Q, Ye H P, Wang S L, Lu Z Y. 2018. A simple automated dynamic threshold extraction method for the classification of large water bodies from Landsat-8 OLI water index images. *International Journal of Remote Sensing*, **39**(11): 3 429-3 451, https://doi.org/10.1080/01431161.2018.1444292.

Zhang W J, Chi W Q, Hu Z J, Liu J Q, Zhang Y Q. 2015. Numerical study on the effect of the Jiaozhou Bay bridge construction on the hydrodynamic conditions in the surrounding sea area. *Coastal Engineering*, **34**(2): 40-50. (in Chinese)

Zhao K, Qiao L L, Shi J H, He S F, Li G X, Yin P. 2015. Evolution of sedimentary dynamic environment in the western Jiaozhou Bay, Qingdao, China in the Last 30 Years. *Estuarine*, *Coastal and Shelf Science*, **163**: 244-253, https://doi.org/10.1016/j.ecss.2014.12.011.